

23 April

Effect of Annealing on Transport Properties of MgO-based Magnetic Tunnel Junctions

A.N. Chiaramonti,^{1,a)} D.K. Schreiber,^{1,2} W.F. Egelhoff,³ D.N. Seidman,² and A.K. Petford-Long¹

¹Materials Science Division, Argonne National Laboratory, Argonne, Illinois 60439

²Materials Science & Engineering Department, Northwestern University, Evanston, Illinois 60208

³Magnetic Materials Group, National Institute of Standards and Technology, Gaithersburg, Maryland 20899-8552

Submitted XX April, 2008

Abstract

The effect of annealing on the transport behavior of CoFe/MgO/CoFe magnetic tunnel junctions has been studied using a combination of site-specific in-situ transmission electron microscopy and three-dimensional atom probe tomography. Annealing at 340 °C for 1 hour in vacuum led to an increase in the resistance of the junctions as compared to the as-grown films. A shift in the conductance curve minimum from zero volts for the as-grown specimen could be correlated with the presence of a CoFe oxide at the lower ferromagnet-barrier interface. The conductance curve for the annealed specimen, however, was found to be symmetric about zero volts. Annealing decreased the asymmetry in the conductance by making the tunnel barrier more homogeneous chemically. This occurred as a result of the diffusion of Co and Fe into the barrier from both the top and bottom ferromagnetic layers.

Introduction

Transport behavior in magnetic tunnel junctions (MTJs) is of great interest both because of the novel properties that are observed, and also because of the potential for integration into a range of technological applications. In the simplest case, MTJs consist of a thin electrically insulating layer

^{a)} Author to whom correspondence should be addressed. Electronic mail: chiaramonti@anl.gov.

23 April

sandwiched between two ferromagnetic electrodes. The resistance of the junction depends upon the relative orientation of the magnetization in the two ferromagnetic layers and the tunneling magnetoresistance (TMR) ratio, which is the output signal measured for the device, is defined as the ratio of the change in resistance when the electrodes are in the parallel versus antiparallel configuration to the resistance in the parallel configuration. Theory predicts TMR ratios of up to 1000% or more for epitaxial MgO-based MTJs, but the current state-of-the-art experimental values reach only half that number. Despite their successful integration into magnetic read heads and magnetoresistive random access memory (MRAM), to date many of the details of the magnetotransport properties, including the exact contribution of interfaces and defects, are not well understood.

It is well known that vacuum annealing treatment can have a major effect on the magnetotransport properties of CoFe-based MTJs. Parkin et al. reported an increase in TMR with annealing temperature up to about 400° C for sputter deposited CoFe/MgO/CoFe MTJs, for junctions that did not fail before reaching that temperature. The resistance of the functioning junctions, however, was found to change little over the same temperature range. This indicates that the mechanisms leading to an increase in TMR with annealing temperature are not necessarily the same as those that result in an increase in resistance. An increase in spin polarization may be part of the reason for such an observation: Wang et al. observed that annealing increased the spin polarization of a CoFe/MgO(001)/CoFe MTJ. Absolute temperature is not the only factor when considering the effects of annealing on MTJs, as it has been shown that optimum TMR can be reached by annealing at lower temperatures for longer times.

23 April

In this paper an analysis is presented of the effect of annealing on the local transport behavior of sputtered CoFe/MgO-based magnetic tunnel junctions using a novel *in-situ* transmission electron microscopy (TEM) technique that combines high spatial resolution imaging with site-specific transport characterization. Three-dimensional atom probe tomography (APT) was employed to elucidate the chemical composition of the layers in three dimensions, at sub-nanometer resolution, and to identify the presence of any unexpected phases.

EXPERIMENTAL DETAILS

Simple MgO-based MTJs were deposited onto boron-doped high conductivity Si(100) ($\rho < 0.001 \text{ } \Omega\text{-cm}$), resulting in a structure of form: Si substrate/Cr seed(5 nm) / $\text{Co}_{50}\text{Fe}_{50}$ (5 nm) / MgO(2 nm) / $\text{Co}_{50}\text{Fe}_{50}$ (10 nm) / Cr cap(60 nm). The metal films were grown by DC magnetron sputtering in 0.4 Pa Ar (3 mTorr), and the MgO was deposited by reactive deposition of Mg metal in a background pressure of 10^{-3} Pa O_2 (10^{-5} Torr) to a nominal thickness of 2 nm. Specimens were examined in the as-grown state and after annealing at 340° C for 1 hr in a vacuum of $4.6 \times 10^{-5} \text{ Pa}$ ($3.5 \times 10^{-7} \text{ Torr}$). Specimens for *in-situ* TEM transport measurements were prepared by FIB milling with a final thickness in the direction of the electron beam of approximately 100 nm. The 60 nm thick Cr cap that was sputter-deposited during the initial sample growth acted as a protective metallization layer to prevent damage to the sample from normally-incident Ga ions. Any FIB-induced damage that did occur was visible in the images collected at the transport measurement sites and therefore was a part of the microstructure to be correlated to the transport data, and could be accounted for in the measurements. Current-voltage (*I-V*) characteristics were measured *in-situ* in the TEM using a nanobiasing TEM holder as described in more detail in Ref. 9. A 4-point probe DC method in voltage sourcing mode was used; the probe tip was an electropolished gold wire with

23 April

a final polished diameter of 100 nm, which was contacted within the specimen thickness and remained relatively constant in shape and size throughout the measurements. Variations due to contact resistance were therefore minimal. Variations in the I - V characteristics along the length of the barrier parallel to the layers can thus be ascribed to differences in the barrier parameters, with the localization of the measurement attributed to ballistic transport. The source of ballistic electrons in this experiment is believed to be the very thin oxide layer on the surface of the TEM specimen, which can be thought of as a tunnel barrier with negligible height that acts as a filter, blocking electrons with a strong transverse momentum component.

Separate specimens suitable for high-resolution electron microscopy (HREM) were prepared by mechanical thinning followed by Ar⁺ ion-milling. APT specimens were prepared using a FIB lift-out method as described in Ref. 10. APT analysis was performed with a local electrode atom probe in laser pulsing mode at 60 K. The estimated accuracy of the resistance measurements is $\pm 1\%$.

RESULTS AND DISCUSSION

Figure 1a shows site-specific I - V curves recorded in-situ in the TEM, for both as-grown (\blacklozenge) and annealed (\bullet) CoFe/MgO/CoFe MTJs. A decrease in the tunneling current at a given voltage following annealing indicates an increase in resistivity. An in-situ TEM image of the as-grown specimen, recorded at the position at which the as-grown I - V curve was measured, is shown in Figure 1b. The tunnel barrier shows light contrast and runs horizontally across the center of the image; it is sandwiched on either side by the FM electrodes that show darker contrast. The contrast within the tunnel barrier is non-uniform and there is a layer showing intermediate contrast at the lower FM/MgO interface. By comparison, the TEM image for the annealed specimen (Fig. 1c)

23 April

shows more uniform contrast in the barrier. Local barrier height and width values were extracted from the experimental transport data by fitting to a suitable model for tunneling through an insulating barrier, for example that of Simmons.¹¹ The Simmons model is an oversimplification and not necessarily phenomenologically accurate for rough barriers or local measurements, however it naturally fits I-V characteristics, is simple, and can be used as a qualitative metric for comparison. Assuming the area of the junction is roughly equal to the square of the diameter tip diameter, 100 nm for these measurements, the average barrier heights and widths are 1.6 V and 6.6 nm for the as-grown specimen and 1.3 V and 10.3 nm for the annealed specimen.

Figure 2 shows the conductance (dI/dV) curves calculated numerically from the I - V curves shown in Figure 1a. The minimum of the dI/dV curve for the as-grown specimen is offset from 0 V by ~ -75 mV, whereas for the annealed specimen the offset is $\sim +25$ mV. The minimum of the dI/dV curve is offset from 0 V if the barrier is asymmetric, and the magnitude of the offset is proportional to the magnitude of the asymmetry as defined as the difference in barrier height at the top and bottom interfaces ($\Delta\phi$). When the average barrier width and height from the Simmons model together with the conductance minimum offset are input into BDR model,¹¹ to calculate the value of the asymmetry, $\Delta\phi$ is approximately 1 V for the as-grown and 0.5 V for the annealed case.

In order to elucidate the origin of the observed shift in the conductance minimum, APT analysis and conventional ex-situ HREM were performed on specimens cut from pieces of the same wafers used for the in-situ TEM studies. The HREM images (Figure 3) clarified the contrast observed in the tunnel barriers of the in-situ images and allowed the layer thicknesses to be determined. Analysis of APT reconstructions of as-grown specimens revealed that the intermediate contrast observed at the

23 April

lower FM metal/MgO interface originates from a layer of CoFe-oxide. A one-dimensional concentration profile through the APT data, taken from a 12 nm diameter cylindrical region normal to the layer interfaces, is shown in Figure 4a. A sharp delineation between the MgO barrier, the CoFe oxide layer and the metallic lower electrode is seen. The Mg:O ratio within the barrier is not stoichiometric 50:50, but closer to 60:40: this is likely a direct result of the reactive sputter deposition parameters, which have led to oxygen diffusing into the lower CoFe electrode. A concentration profile obtained in the same manner from the annealed specimen, Figure 4b, shows interdiffusion of the top and bottom FM layers into the MgO barrier, with Fe diffusing more readily than Co. Mg and O have diffused from the barrier into the bottom FM layer, with O diffusing further than Mg. The mixed CoFe oxide at the bottom FM/tunnel barrier interface is still present, but all of the interfaces are considerably more diffuse than for the as-grown specimen. Isoconcentration surfaces (isosurfaces) at the bottom CoFe/CoFe oxide interface of the as-grown and annealed samples, taken at 15 at.% oxygen, show that oxygen has diffused into the bottom CoFe layer preferentially via grain boundaries. A comparison of the average mass density calculated from the APT composition profile with the mass contrast observed in the HREM images, showed good agreement for both as-grown and annealed specimens.

The barriers in both the as-grown and annealed specimens are asymmetric, however the magnitude of the asymmetry in the as-grown specimen is much greater. This is due to the fact that the layers in the as-grown sample are compositionally distinct and sharply defined, and the MgO barrier is surrounded on one side by CoFe and the other by CoFe oxide. The barrier region in the annealed specimen, although more interdiffused, is more symmetric. The barrier height has decreased slightly which is consistent with a change from relatively pure MgO to (MgO + Fe,Co). The barrier width

23 April

has increased, suggesting that some of the CoFe oxide layer, for example the part containing Mg metal, may now be contributing to the tunnel barrier. The remaining small difference in barrier height between the top and bottom interfaces for the annealed specimens may be due to the thinner region of CoFe oxide at the bottom interface that persists upon annealing.

This manuscript has been created by UChicago Argonne, LLC, Operator of Argonne National Laboratory. Argonne, a U.S Department of Energy Office of Science Laboratory, is operated under contract No. DE-AC02-06CH11357. The electron microscopy was accomplished in the Electron Microscopy Center for Materials Research at Argonne National Laboratory. Three-dimensional atom probe tomography was carried out at the Northwestern University Center for Atom Probe Tomography (NUCAPT).

References

- [1] S. Parkin, X. Jiang, C. Kaiser, A. Panchula, K. Roche, and M. Samant (2003) Proc. IEEE 91, 661–679.
- [2] W.H. Butler, X.G. Zhang, T.C. Schulthess, and J.M. MacLaren (2001) Phys. Rev. B 63, 5, 054416:1–12.
- [3] J. Mathon, and A. Umerski (2001) Phys. Rev. B 63, 220403:1–4.
- [4] J. Hayakawa, S. Ikeda, Y.M. Lee, F. Matsukura, and H. Ohno (2006) Appl. Phys. Lett. 89, 232510:1–3.
- [5] J-G. Zhu and C. Park (2006) Materials Today 9, 36–45.
- [6] S.S.P. Parkin, C. Kaiser, A. Panchula, P.M. Rice, B. Hughes, M. Samant, and S.-H. Yang (2004) Nature Materials 3, 862–867.
- [7] R. Wang, X. Jiang, R.M. Shelby, R.M. Macfarlane, S.S.P. Parkin, S.R. Bank, and J.S. Harris (2005) Appl. Phys. Lett. 86, 052901:1–3.
- [8] T. Dimopoulos, G. Gieres, J. Wecker, N. Wiese, Y. Luo, and K. Samwer (2005) J. Appl. Phys. 98, 073705:1–5.
- [9] A.N. Chiamonti, L.J. Thompson, W.F. Egelhoff, and A.K. Petford-Long (2008) Ultramicroscopy , In–press.
- [10] K. Thompson, D. Lawrence, D.J. Larson, J.D. Olson, T.F. Kelly, and B. Gorman (2007) Ultramicroscopy 107, 131–139.
- [11] J.G. Simmons (1963) J. Appl. Phys. 34, 1793–1803.
- [12] W.F. Brinkman, R.C. Dynes, and J.M. Rowell (1970) J. Appl. Phys. 41, 5, 1915–1921.

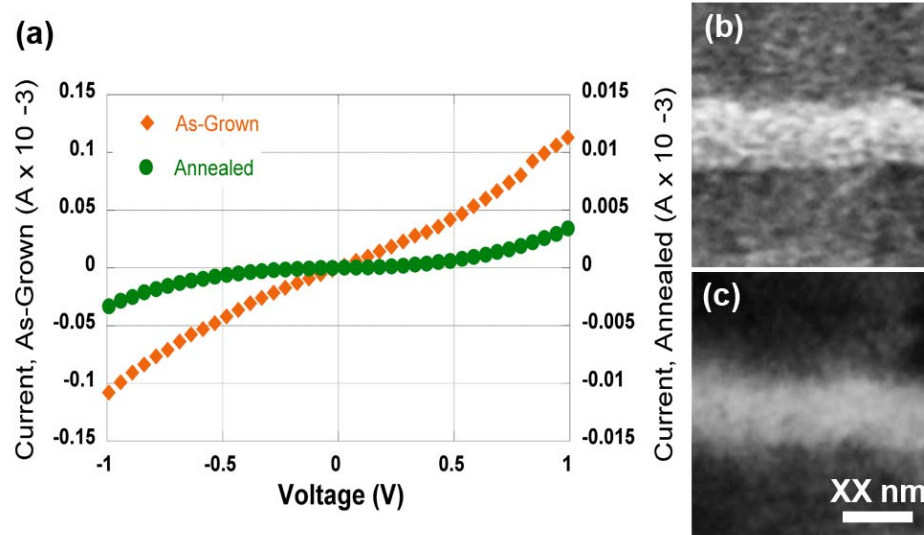
Figures & Figure Captions:

Figure 1 (a) In-situ site specific current-voltage characteristics for a CoFe/MgO/CoFe MTJ in both the as-grown (\blacklozenge) and annealed at 340 °C for 1 h state (\bullet). *In-situ* TEM images for the (b) as-grown and (c) annealed specimens, corresponding to the I-V curves in (a). The TEM images are small representative sections of a larger image corresponding to area probed by the 100 nm diameter tip.

23 April

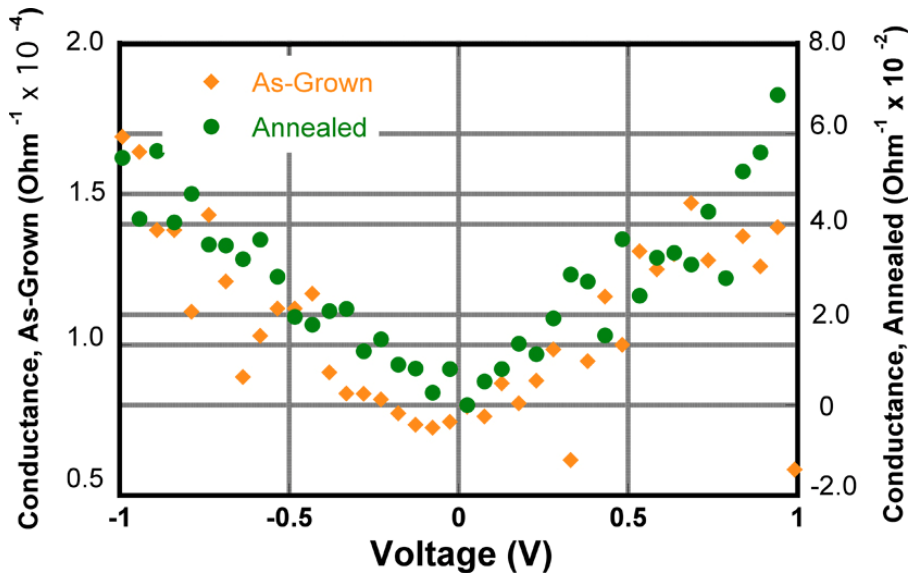


Figure 2: Numerically derived conductance (dI/dV) curves from the I-V curves in Figure 1. The minimum of the as-grown curve (\blacklozenge) is shifted from 0 V by -75 mV while the annealed curve (\bullet) is shifted by only +25 mV.

23 April

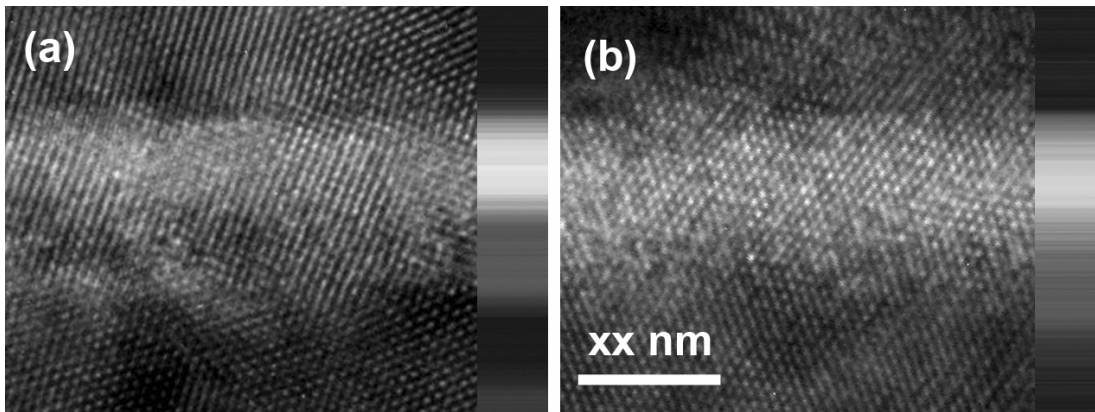


Figure 3: *Ex-situ* HREM images of (a) as-grown and (b) annealed CoFe/MgO/CoFe MTJ.

Superimposed on each image is a spectrum of the average mass density as a function of position through the barrier calculated from the APT 1-D composition profile on an absolute scale. The mass contrast in the TEM images agrees with that calculated from the APT reconstruction.

23 April

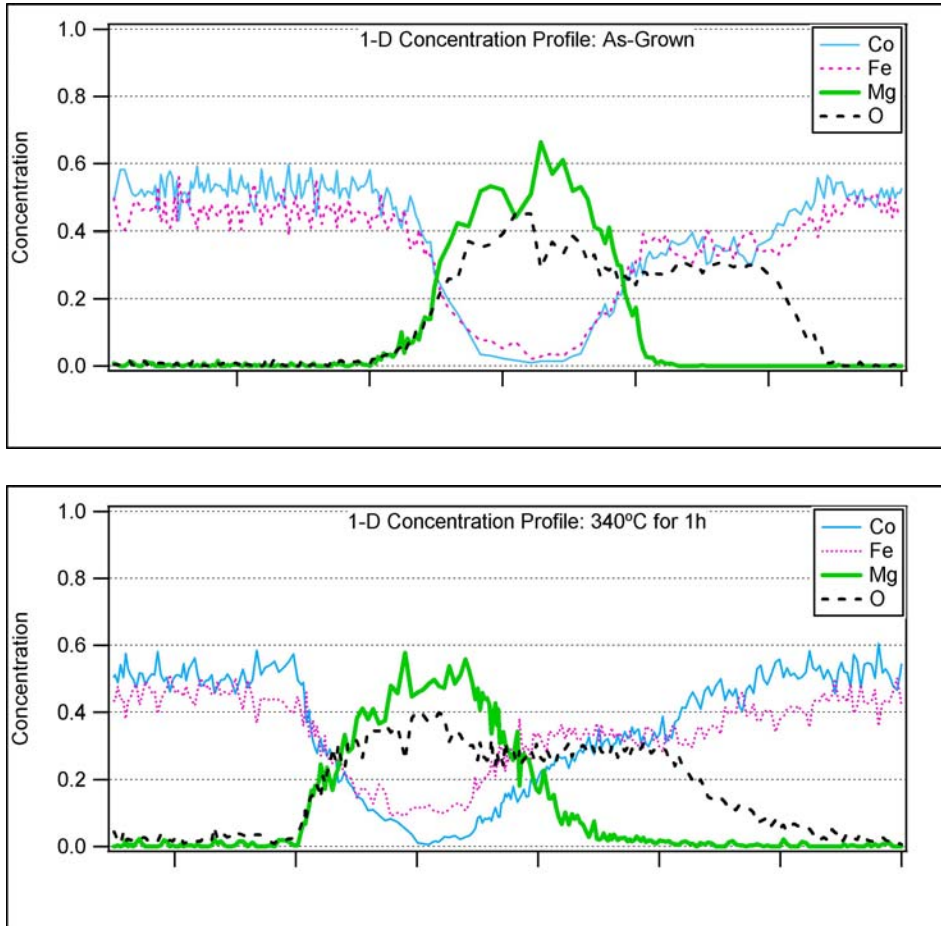


Figure 4: One-dimensional concentration profiles from APT of (a) as-grown and (b) annealed samples. In the as-grown profile, the interfaces between the CoFe/CoFe-oxide/MgO/CoFe are relatively sharp. Upon annealing (b) the interfaces are much more diffuse, with Co and Fe penetrating the MgO, Mg into the CoFe-oxide and O into the bottom CoFe.